Dynamic Stress Intensity Factors of Brittle Materials

ALBERT S. KOBAYASHI and KWAN HO YANG
University of Washington, Department of Mechanical Engineering, Seattle, Washington 98195, USA

ABSTRACT

A new hybrid experimental-numerical procedure was used to characterize dynamic fracture response of structural ceramics at elevated temperature. The dynamic stress intensity factor (SIF) versus crack velocity relations of glass and reaction bonded silicon nitride (RBSN), which were obtained by the first author and his colleagues, are reviewed. The dynamic SIF versus crack velocity relations of alumina, TiB_2-particulate/SiC-matrix composite and SiC_w/Alumina-matrix composite are also presented. Available data indicated that dynamic arrest SIF was not observed in glass and monolithic ceramics, and suggested that further studies be conducted to resolve the existence or lack of existence of a dynamic arrest SIF in ceramic matrix composites.

KEYWORDS

Dynamic fracture testing; hybrid experimental-numerical procedure; dynamic stress intensity factor; crack opening displacement; glass; reaction bonded silicon nitride; alumina; TiB_2-particulate/SiC-matrix composite, SiC_w/alumina-matrix composite.

INTRODUCTION

Historically the destiny of dynamic fracture mechanics was set with the pioneering experimental analysis of Wells and Post (1958) augmented by Irwin's data analysis in 1958 (Irwin 1958). Since that time, numerous attempts have been made to relate the crack velocity with the apparent crack driving force which in most cases were considered synonymous with the dynamic stress intensity factor. Having bridged this gap without proof, most of the experimental data, with the authors being no exception, has been reported in terms of the crack velocity versus dynamic fracture toughness relation where the toughness was equated to the driving force from static equilibrium consideration.

Some of the cogent results and the controversies surrounding the above mentioned experimental data were discussed in a recent paper by the authors and their colleagues (Kobayshi et al 1986). In particular, the dynamic stress intensity factors versus crack velocity relations for structural ceramics, i.e. reaction bonded silicon nitride, did not exhibit a tendency for dynamic crack arrest in contrast to the familiar gamma-shaped relations which were routinely observed in dynamic fracture experiments of structural metals and polymers. This

lack of a dynamic crack arrest stress intensity factor, below which the running crack will arrest, in structural ceramics was particularly disturbing. From the viewpoint of fracture mechanics, the highly touted ceramic heat engine would have little chance but shatter in the presence of a critical crack.

The purpose of this paper is to review the past results on dynamic fracture testing on ceramics and to present additional experimental results which have been generated since 1986. A possible explanation for the lack of a dynamic crack arrest stress intensity factor in the structural ceramics will also be presented.

DYNAMIC FRACTURE TESTING OF CERAMICS

Dynamic fracture testing of ceramics differs with that of structural metals and polymers in that the available test specimens are often as small as 6x6x40 mm bars which are dictated by the high fabrication cost and the availability of blank materials. In terms of experimental techniques, the popular optical methods for determining the dynamic stress intensity factors, such as photoelasticity and caustics, cannot be used due to the opaqueness and low Poisson's ratio of ceramics. As for crack length measurements, the traditional photographic and crack gage techniques for monitoring the rapid crack propagation are unusable at elevated temperature and at the best, inaccurate under room temperature usage due to the small crack opening displacements. In addition, under dynamic loading at elevated temperature, the impact load, which must be measured outside of the furnace, could be vastly different from the applied load at the impact point on the specimen. These physical constraints requires the development of new dynamic fracture testing procedures which heretofore was unachievable.

The experimental procedure, which circumvented some of the above difficulties, is the hybrid experimental-numerical procedure in which experimental data, such as the measured crack velocity, is used to drive a well established dynamic finite element code (Kobayashi 1979). The evolution of this hybrid procedure will be discussed together with the experimental results in the following sections.

WL-MTDCB Tests

During the initial stage of development, the commercially available KRAK-GAGE, 25 mm long, was used to monitor the rapid crack extension history during dynamic fracture at room temperature. These tests were conducted with glass and locally fabricated reaction bonded silicon nitride (RBSN) specimens which permitted the luxury of using the experimentally more manageable larger wedge-loaded modified tapered double cantilever beam (WL-MTDCB) specimen with a side groove.

Figure 1 shows the WL-MTDCB specimens and the loading conditions used in the initial phase of this investigation. The measured crack extension and the wedge load histories were input to an implicit dynamic finite element code, which was executed in its generation mode (Kobayashi 1979), to simulate the dynamic fracture test. The work done at the smoothly released crack-tip node, which model gradual crack extension, was used to compute the dynamic stress intensity factor of the moving crack tip. Calibrated crack opening displacements were used to compute the stress intensity factor (SIF) prior to crack extension.

The unusual specimen configuration, which was necessitated by its contemplated use at temperature in excess of 1000°C, as well as the hybrid technique required certification. For this purpose, the dynamic fracture response of 4340 steel hardened to Rockwell C44 was analyzed by using the identical hybrid procedure. Four WL-MTDCB specimens with machined blunt crack tips were statically loaded to failure at room temperature. While the running cracks did not arrest in this series of dynamic fracture tests, crack arrest was observed in this inherently stiff specimen machined from annealed 4340 steel. Figure 2 shows the dynamic SIF versus crack velocity relation (Kobayashi et al. 1986) obtained in this study as

well as that of Rosakis et al (1984). The agreement between the two independent results could be due in part to the similarities in specimen geometries. The prominent vertical stem or the existence of a dynamic crack arrest SIF is also noted.

Figure 3 shows dynamic SIF versus crack velocity relation obtained from two plate glass WL-MTDCB specimens. Also shown are the results obtained from four wedge-loaded, rectangular double cantilever beam (WL-RDCB) specimens. The crack acceleration phase, which was prominently discussed in the early study (Kobayashi et al. 1983), was later attributed to the reduced sensitivity of the KRAK-GAGE in the presence of small crack opening displacement inherent in brittle materials. Thus this initiation phase, which is an experimental artifact, has been eliminated in Fig. 3. These tests are the first of many test results which exhibited continuing crack propagation in the presence of dynamic SIF's much lower than the fracture toughness of the material.

Figure 4 shows the dynamic SIF versus crack velocity relations of two statically and six dynamically loaded, RBSN WL-MTDCB specimens. Again the crack initiation phase, which was described in a previous publication (Liaw et al. 1986), was eliminated. This figure shows that the running crack in the statically loaded WL-MTDCB specimens attempted to arrest at lower dynamic SIF but the dynamically loaded specimens did not show such a trend.

3-Point Bend Tests

While the WL-MTDCB specimens used in the above investigation provided controllable crack propagation in relatively small specimens, these specimens were too costly to fabricate in large quantities. The use of three-point bend specimens in subsequent dynamic fracture testing was thus dictated by the availability of specimen blanks and the relative ease in machining. Figure 5 shows the three-point bend specimens.

The KRAK-GAGE, which appeared to function well in previous room temperature fracture testing, obviously could not be used at the elevated temperature. Therefore, a noncontacting laser interferometric displacement gage (LIDG) (Sharpe 1971) was used in subsequent tests. The relative displacement between the two reflective LIDG targets is determined by the relative movements of two sets of optical interference fringes generated from a coherent light reflected from the microhardness indentations on the targets. Fringe movements due to the changes in the relative distance between the two indentations are monitored by two photomultiplier tubes and recorded by transient recorders. Details of the LIDG technique as applied to fracture testing are found in (Jenkins et al 1987). In this dynamic fracture investigation, the LIDG technique was used to measure the crack opening displacement (COD) at the initial notch tip.

The loading system consisted of a drop weight tower, which is mounted integrally with a furnace, as shown in Fig. 6. The two portholes and one door, which are shielded with fused glass pane to prevent the undesirable convection air current, provided the LIDG access to the fracture specimen. The impact load applied to the specimen is monitored by a load transducer outside of the furnace.

The experimental procedure consisted of relating the measure COD at the initial notch tip to the instantaneous crack length through a calibration curve for a given specimen geometry. Because of small differences in material properties and specimen geometries, these calibration curves had to be generated for each series of specimens shown in Fig. 6. During the course of this calibration, which involved a combined use of the KRAK-GAGE and the LIDG techniques, the KRAK-GAGE was found to be relatively insensitive to the initial phase of crack extension in these brittle materials with small COD's. As shown in Fig. 7, the time lag and the lack of the crack acceleration phase, which was overemphasized in previous studies (Kobayashi et al. 1983; Liaw et al. 1986), in the LIDG established the limitation of the KRAK-GAGE. The acceleration phase was thus eliminated from the Figs. 3 and 4. Further details of this calibration procedure is found in (Kobayashi et al. 1988).

The hybrid analysis based on the above experimentally determined crack extension history required, as an additional input, the applied load history which had to be measured outside of the furnace. Uncertainty in the actual load applied at the load point on the specimen required that the entire loading system, which included the push rod, to be modeled in the dynamic finite element analysis as shown in Fig. 8. This complex modeling required validation which was conducted at room temperature with an additional load measurement at the impact point of the specimen (Kobayashi et al. 1988). Figure 9 shows a typical comparison between the measured and computed load. The loss of contact was established by monitoring the sign of the normal stresses of the two contacting elements in the specimen and the push rod. The dynamic finite element analysis also revealed similar loss of contact at the two end supports and had to be accounted for in subsequent analyses.

The hybrid technique was then used to determine the dynamic SIF versus crack velocity relations of alumina (Kobayashi et al. 1988), TiB_2-particulate/SiC-matrix composite and SiC-whisker/alumina-matrix composite (Jenkins et al. 1988). Figure 10 shows the dynamic SIF versus crack velocity relations of four room-temperature and two 1000°C fracture tests of alumina three-point bend specimens. Notable is the cluster of data points of low velocity crack propagation at dynamic SIF which are less than one half of the static fracture toughness.

Figures 11 and 12 show the dynamic SIF versus crack velocity relations for the two ceramic composites of TiB_2-particulate/SiC-matrix and SiC-whisker/alumina matrix, respectively. At the time of this writing, the data for the low dynamic SIF region of the former is missing and more data is sought for the latter.

DISCUSSION

The unambiguous absence of the dynamic crack arrest SIF in the monolithic glass, RBSN and alumina was not obvious in the ceramic composites considered. As shown in Fig. 13, the propagating crack in a SiC-whisker/alumina-matrix, three-point bend specimen, which was loaded under fixed grip condition, arrested at 1200° C (Jenkins et al 1988). Thus, the existence of a dynamic crack arrest SIF is a possibility which requires further study.

CONCLUSIONS

A hybrid procedure for determining the dynamic SIF associated with a running crack in three-point bend specimens at elevated temperature was established.

This procedure was used to determine the dynamic SIF versus crack velocity relations of glass, reaction bonded silicon nitride, alumina, TiB_2-particulate/SiC-matrix composite and SiC-whisker/alumina-matrix composites.

Dynamic crack arrest SIF was not observed in glass and monolithic ceramics.

ACKNOWLEDGEMENT

The results reported here were generated under NASA contract NAGW-199.

REFERENCES

Wells, A.A. and D. Post, (1958). Proceedings of the Society for Experimental Stress Analysis, Vol. XVI, No. 1 69-92.

Irwin, G.R.(1958), Proceedings of the Society for Experimental Stress Analysis, Vol. XVI, No. 1 93-96.

Kobayashi, A.S., M. Ramulu, M.S. Dadkhah, K.-H. Yang and B.S.-J. Kang, (1986). International Journal of Fracture, Vol. 30 275-285.

Kobayashi, A.S., (1979). Nonlinear and Dynamic Fracture Mechanics, ed. N. Perrone and S.N. Atluri, ASME AMD 35 19-36.

Rosakis, A.J., J. Duffy and L.B. Freund, (1984). Journal of the Mechanics and Physics of Solids, Vol 32, No. 4 443-460.

Kobayashi, A.S., A.F. Emery and B.M. Liaw, (1983). Fracture Mechanics of Ceramics, Vol. 6, ed. R.C. Bradt, A.G. Evans, D.P.H. Hasselman and F.F. Lange, Plenum Publishing Corp. 47-61.

Liaw, B.M., A.S. Kobayashi and A.F. Emery, (1986). Fracture Mechanics: Seventeenth Volume, ASMT STP 905, ed. J.H. Underwood, R. Chait, C.W. Smith, D.P. Wilhelm, W.A. Andrews and J.C. Newman 95-107.

Sharpe, Jr., W.N., (1971). International Journal of Nondestructive Testing, Vol. 3, 59-76.

M.G. Jenkins, A.S. Kobayashi, M. Sakai, D.W. White and R.C. Bradt, (1987). American Ceramic Society Bulletin, Vol. 12, No. 66 1734-1738.

Kobayashi, A.S. and K.-H. Yang, (1988). To be published in the Proceedings of International Conference on Advanced Measurement Techniques, British Society for Strain Measurements.

Kobayashi, A.S., K.-H. Yang and A.F. Emery, (1988). To be published in IMPACT 87, Deutsch Gesellschaft fuer Metallkunde.

Jenkins, M.G., A.S. Kobayashi, K.W. White and R.C. Bradt, (1988). To be published in Engineering Fracture Mechanics.

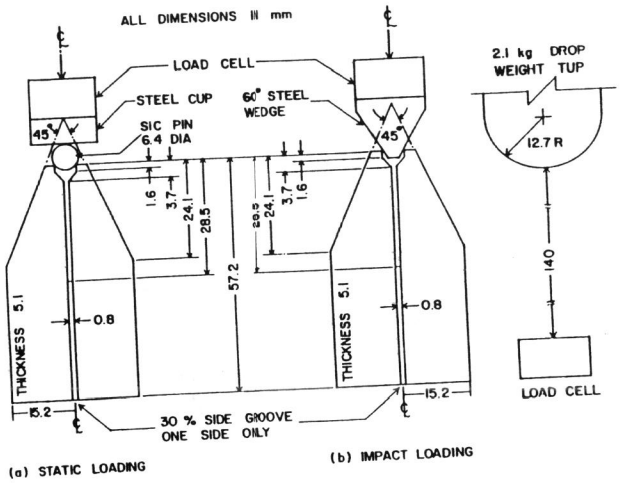

Fig. 1. WL-MTDCB RBSN Specimen.

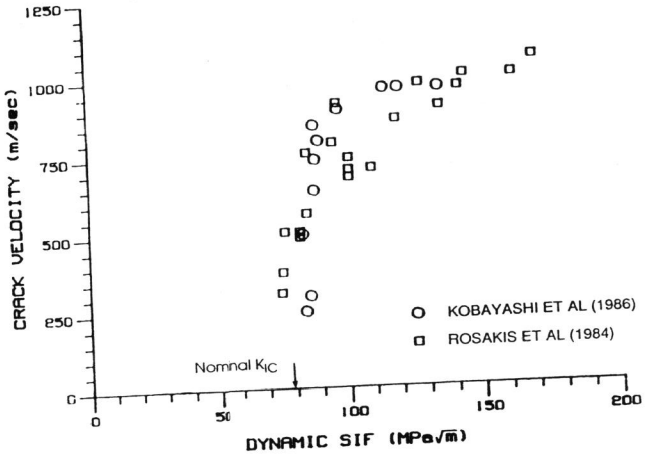

Fig. 2. Dynamic SIF Versus Crack Velocity Relation,.4340 Steel

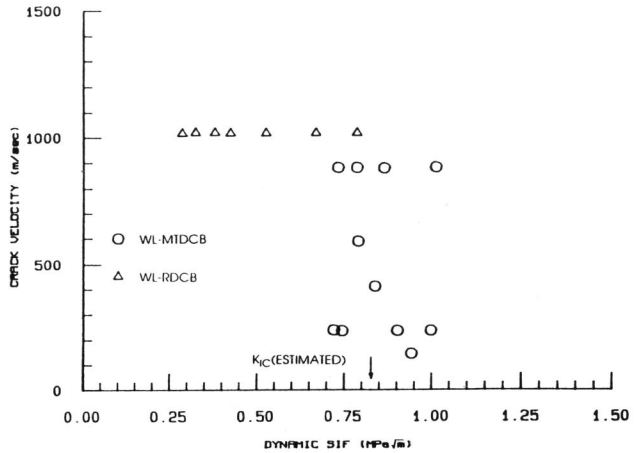

Fig. 3. Dynamic SIF Versus Crack Velocity Relation, Glass.

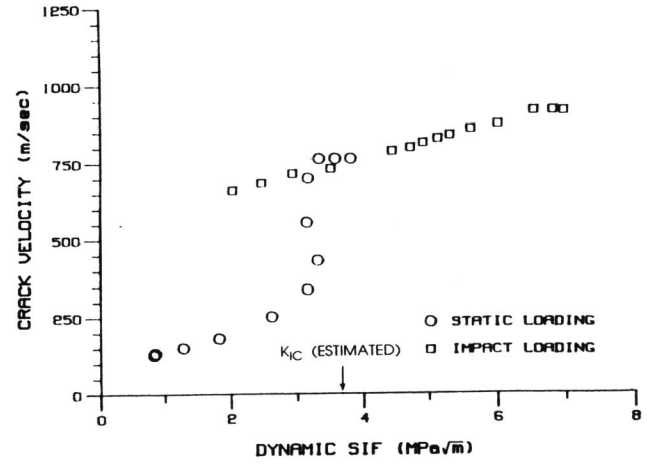

Fig. 4. Dynamic SIF Versus Crack Velocity Relation,.Blunt Notch RBSN WL-MTDCB Specimens

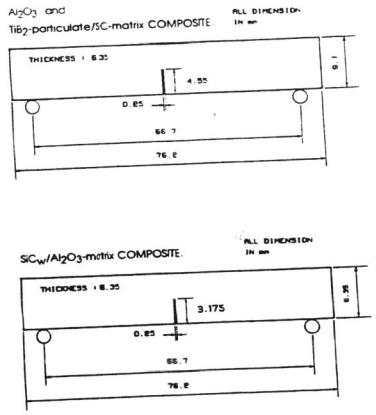

Fig. 5. 3-Point Bend Specimens.

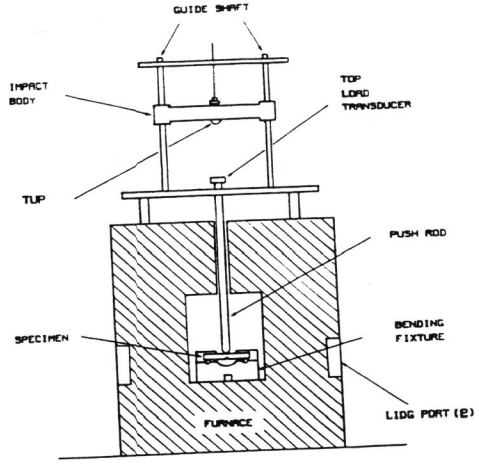

Fig. 6. Schematic Diagram of Drop-Weight Impact and Furnace with LIDG Ports.

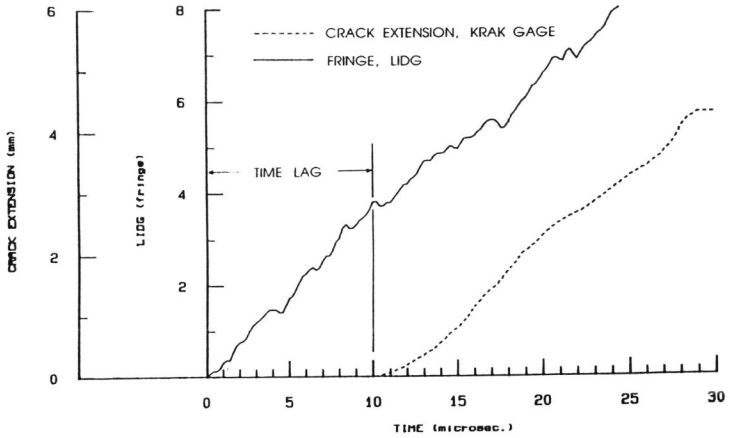

Fig. 7. LIDG Data and Crack Extension Data, TiB_2-particulate/ SiC-matrix Composite (HE121487).

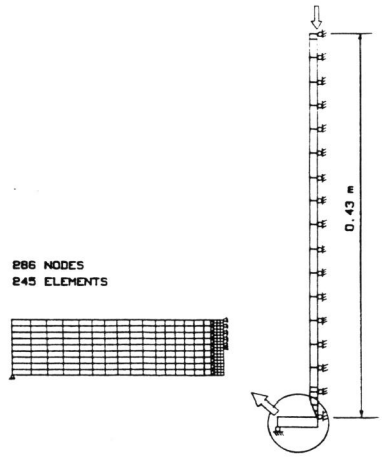

Fig. 8. Finite Element Breakdown.

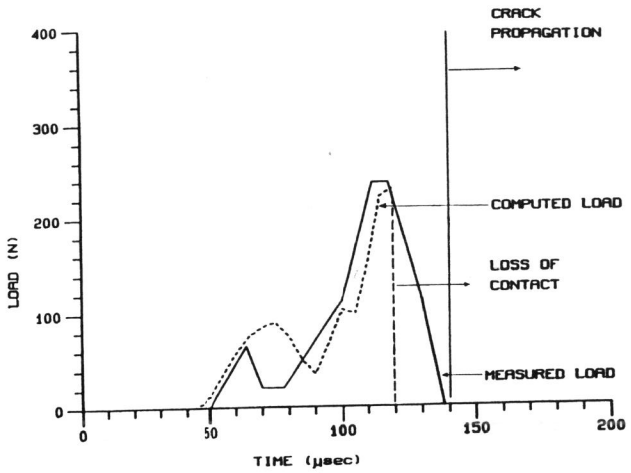

Fig. 9. Comparison of Measured and Computed Load Traces, Alumina (KH021887)..

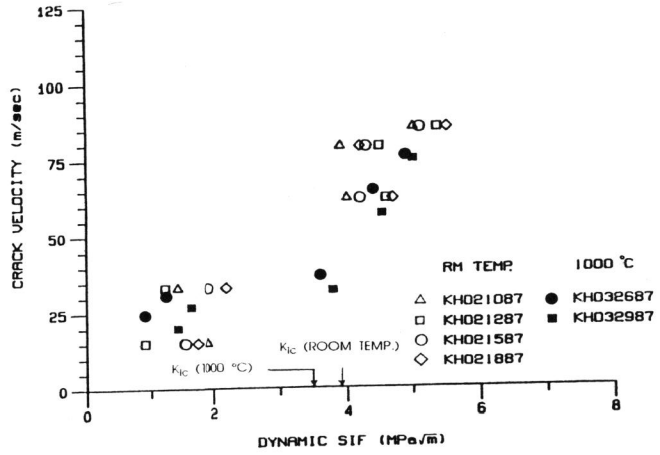

Fig. 10. Dynamic SIF Versus Crack Velocity Relation, Alumina.

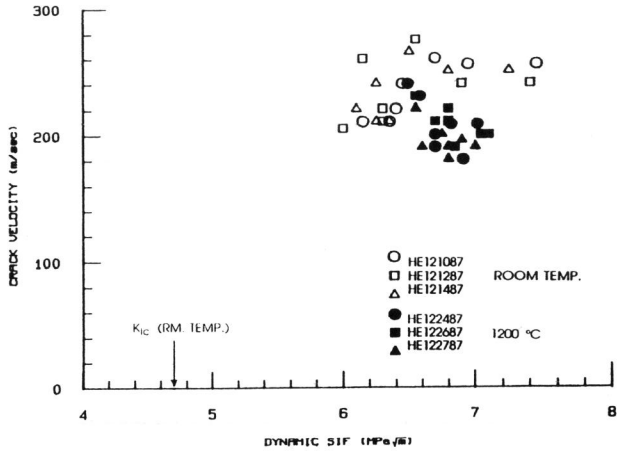

Fig. 11 Dynamic SIF Versus Crack Velocity Relation at Room and 1200°C Temperatures. TiB_2-particulate/SiC-matrix Composite.

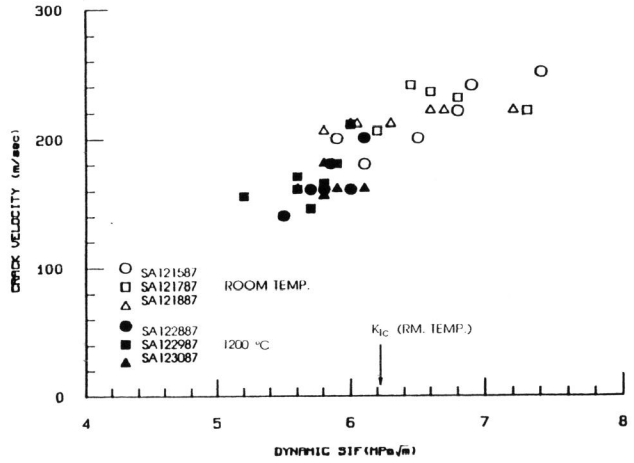

Fig. 12. Dynamic SIF Versus Crack Velocity Relation at Room and 1200°C Temperatures. SiC_w/Al_2O_3-matrix Composite.

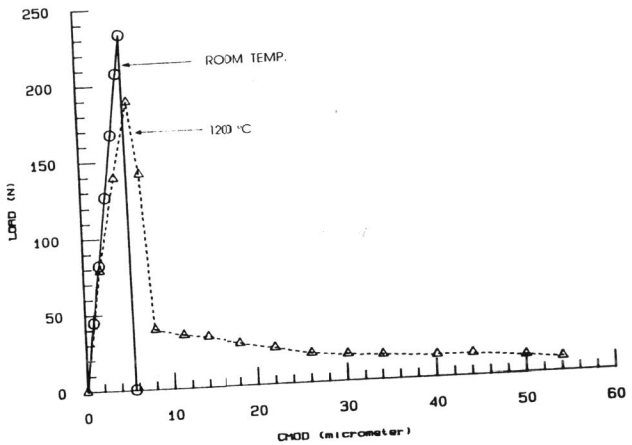

Fig. 13. Representative Load Versus Crack Mouth Opening Displacement(CMOD) Histories for SiC Whisker/Al_2O_3-Marix Composite Three-Point Bend Specimens.